HHS Public Access

Author manuscript

ACS Sens. Author manuscript; available in PMC 2026 July 14.

Published in final edited form as:

ACS Sens. 2026 June 26; 11(6): 4960–4970. doi:10.1021/acssensors.6c00882.

Modular Input–Output Biosensor Design Using *De Novo* Protein Switches

James Wang[†],
Department of Biomolecular Engineering, University of California, Santa Cruz, California 95064, United States

Julie Yi-Hsuan Chen[†],
Department of Biomolecular Engineering, University of California, Santa Cruz, California 95064, United States

Chenggang Xi[†],
Department of Biomolecular Engineering, University of California, Santa Cruz, California 95064, United States

Estrella Arteage-Organiz,
Department of Biomolecular Engineering, University of California, Santa Cruz, California 95064, United States

Andy Hsien-Wei Yeh
Department of Biomolecular Engineering, University of California, Santa Cruz, California 95064, United States; Genomics Institute, University of California, Santa Cruz, California 95064, United States

Abstract

Protein-based biosensors offer unique advantages over conventional analytical methods by enabling real-time detection of target analytes with minimal sample preparation. However, efficiently coupling molecular recognition to a reliable output signal remains a key challenge in biosensor design. Here, we present a plug-and-play strategy using the *de novo* switch platform, LOCKR, which enables direct transduction of a binding event into a defined signal output. The LOCKR architecture supports modular reconfiguration: the recognition domain can be swapped to detect a desired analyte, while the reporter module can be interchanged to tune the output format. We expand the range of LOCKR-compatible readouts beyond split luciferase to include ratiometric Förster-type resonance energy transfer and β-lactamase-based colorimetry.

Corresponding Author: Andy Hsien-Wei Yeh – Department of Biomolecular Engineering, University of California, Santa Cruz, California 95064, United States; Genomics Institute, University of California, Santa Cruz, California 95064, United States; hsyeh@ucsc.edu.

[†]J.W., J.Y.-H.C., and C.X. contributed equally.

Author Contributions

A.H.-W.Y. conceived, conceptualized, and supervised the project. J.W. and J.Y.-H.C. carried out *in vitro* biosensor characterization with the help of E.A.O., J.Y.-H.C., C.X., J.W., and A.H.-W.Y. processed and analyzed the data. C.X. prepared the schematics and carried out the reversibility assays. A.H.-W.Y. wrote the initial manuscript, and all authors revised the final manuscript.

Complete contact information is available at: https://pubs.acs.org/doi/10.1021/acssensors.6c00882

A.H.-W.Y. is a coinventor in several patent applications covering the LOCKR platform.

By integrating computationally designed high-affinity binders as interchangeable recognition elements, we demonstrate sensitive detection of glucagon, neuropeptide Y, and peptide YY with limits of detection in the picomolar range. Together with the expanding landscape of *de novo* designed binders and reporters, the LOCKR platform bridges the gap between molecular recognition and signal generation, enabling versatile biosensor development tailored for user-defined applications.

Graphical Abstract

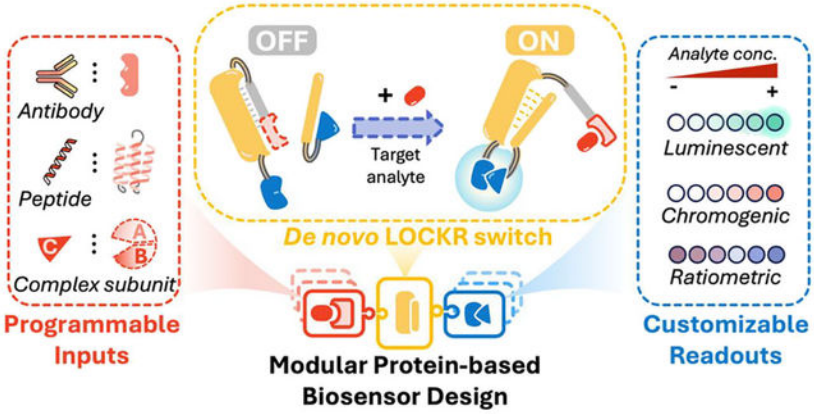

Keywords

protein design; protein switch; biosensor; reporter; bioassay

Protein-based biosensors are engineered biomolecular switches that can detect specific target analytes and transduce recognition events into measurable signals. Over the past few decades, such biosensors have enabled real-time monitoring of cellular states,[1] *in vivo* physiology,[2] and biomarker levels.[3] Typically, these biosensors consist of two core modules: a recognition domain, which selectively binds the analyte of interest, and a reporter domain, which generates a detectable output (e.g., fluorescence, luminescence, or chromogenic activity) upon analyte binding. Traditionally, efficient coupling of target recognition to signal production often relies on less predictable protein conformational changes and thereby typically requires empirical optimization, such as tuning linker lengths, domain orientations, permutations, or point mutations.[4–8] In recent years, advances in deep learning have markedly expanded the ability to design *de novo* proteins with tailored functions,[9,10] including binders for target recognition[11–13] and enzyme reporters for signal generation.[14,15] Leveraging the modularity and geometrically compatible nature of *de novo* proteins,[16] we reasoned that a *de novo* switch architecture could serve as a generalizable platform for converting binder engagement into a defined conformational change that can then be coupled to enzymatic reporter activation. Such a platform could enable the modular input–output design, offering an orthogonal and tunable mechanism to translate target binding into a user-defined output signal. Previously, the Baker lab computationally designed the LOCKR (Latching Orthogonal Cage–Key pRotein) protein switch system.[17,18] In this system (Figure 1A), a “Cage” protein uses a “Latch” domain to hold a target

recognition domain in an inactive conformation (“OFF” state). Upon binding to a cognate “Target” protein, the system undergoes a conformational change that permits the complex to engage in a Cage–Key association with a separate “Key” protein, shifting into the open conformation (“ON” state). The three-component equilibrium can be thermodynamically linked to a reporter output for generating a measurable Förster-type resonance energy transfer (FRET) signal[19] or to an effector in cells.[20] In our prior implementation to build biosensors for *in vitro* diagnostics,[21] we used a split luciferase complementation system within the LOCKR architecture, enabling the detection of antibodies, viral proteins, protein complex subunits, and antibodies. The overall response is tunable with high specificity for the cognate target while providing a rapid, homogeneous, all-in-solution, and sensitive readout suitable for *in vitro* diagnostics[22] (Figure 1B).

Building on this foundation, we aim to extend the LOCKR architecture in two modular directions to demonstrate its versatility as a programmable input–output conversion system. First, we broaden the reporter module beyond split luciferases by implementing luciferase-driven bioluminescence Förster-type resonance energy transfer (a.k.a., BRET) or a β-lactamase-based colorimetric readout, showing that the same protein switch can be coupled to multiple orthogonal signal-transduction modalities (Figure 1A). Second, we extend the recognition module beyond previous collections[21] by incorporating recently developed high-affinity *de novo* designed helical binders as sensing domains to detect clinically relevant peptides, including glucagon (GCG), neuropeptide Y (NPY), and peptide YY (PYY). Together, these advances establish LOCKR as a modular framework in which inputs and outputs can be independently reprogrammed while preserving core features of *de novo* proteins (Figure 1B), including low-cost production, broad modularity, and high stability.

RESULTS AND DISCUSSION

Design of a Ratiometric HBV Antibody Biosensor via Intramolecular BRET

Luciferase-catalyzed chemiluminescence generally provides greater sensitivity than fluorescence in biological matrices because it avoids excitation-dependent autofluorescence and interference in whole-blood samples that limit quantitative measurements.[23] However, absolute luminescence intensity is known to be affected by the matrix effects in serum or whole-blood samples.[6] To mitigate this, BRET biosensors can produce an internally normalized signal by reporting the ratio of luminescence emissions at two distinct wavelengths, which reflects the changes of energy transfer efficiency between the donor and acceptor fluorophores.[6,24] This ratiometric signal is independent of absolute luminescence decay and provides greater robustness across varying sample conditions. Previous studies showed that such BRET biosensors function more reliably in various complex biological fluids and matrices.[25–27] Transitioning our intensiometric biosensors to a ratiometric BRET format would therefore potentially enhance the quantitative utility. To implement a ratiometric readout in the LOCKR platform, we designed an intramolecular BRET configuration by fusing teLuc[28] (donor) to the N-terminus and CyOFP[29] (acceptor) to the C-terminus of the Cage protein (Figure 2A). When in the OFF state, the two termini of the Cage protein are in close three-dimensional proximity, enabling high donor–acceptor BRET efficiency. Upon target binding, the Cage–Key–Target thermodynamic equilibrium shifts the

conformational ensemble toward the open state, increasing the donor–acceptor distance and thereby reducing BRET efficiency.

As a proof of concept, we validated this intramolecular BRET reporter module in our previous lucCageHBV LOCKR biosensor for hepatitis B virus (HBV) antibody detection as the template.[21] We first computationally threaded in a second HBV epitope (ANSNNPDWDF)[30] into the Latch of lucCageHBV to promote HBV antibody-epitopes binding with bivalent interactions, providing sufficient thermodynamic driving force (ΔG_{BT}) to open the Cage (Figure 2A). To validate the OFF-state BRET efficiency, we evaluated constructs with progressive N-terminal truncations of CyOFP to vary the distance between the Latch and CyOFP domains. Consistent with our design models, shorter Latch–CyOFP distances correlated with higher baseline BRET efficiencies (Figure 2B), supporting the spatial orientation and geometry of the donor–acceptor in the OFF state. We selected construct B0622_d6, containing a six-residue truncation at the N-terminus of CyOFP and exhibiting a higher BRET dynamic range, for further analysis. Upon titration with HBV antibody, the biosensor exhibited a dose-dependent response in a thermodynamic equilibrium manner, achieving a ~207% ratiometric change (Figure 2C) while maintaining a low-nanomolar limit of detection (LOD). The color hue shifted from reddish (w/ low concentration of the HBV antibody) to bluish (w/ high concentration of the HBV antibody) and could be captured by a smartphone camera, supporting the feasibility of app-based quantification using calibrated RGB ratios or integration into paper-based analytical devices.[31]

Design of a Colorimetric Troponin I Biosensor via Split β-Lactamase

Colorimetric absorbance-based biosensors offer another simple and equipment-free option for assay detection, as they produce visually interpretable signals that can be read by the naked eye. To incorporate a colorimetric readout into the LOCKR platform, we utilized split β-lactamase[32] as the output reporter, in which target-induced Cage–Key association reconstitutes enzymatic activity and enables substrate turnover (Figure 3A). Reconstituted β-lactamase can hydrolyze the chromogenic nitrocefin substrate that undergoes a color change from yellow to red upon cleavage. Since the hydrolyzed product accumulates over time in solution, this system functions as an end-point assay in which greater enzyme activity leads to faster color change. To maximize the performance, an important design insight is to suppress background activity in the OFF state, as low-level leakage can lead to false positives.

As a proof of concept, we fused the split β-lactamase components to the previously designed lucCageTrop[21] biosensor for human cardiac troponin I (cTnI) detection, a biomarker for acute myocardial infarction (AMI). In this system (Figure 3A), the split β-lactamase chain A (LacA) was genetically fused to the N-terminus of Cage (LacA_lucCageTrop), while the chain B (LacB) was fused to the C-terminus of Key (MBP_key_LacB). In the absence of cTnI, the biosensor remains in the OFF state and prevents split β-lactamase reassembly. Upon cTnI binding, the biosensor transitions to the ON state, which promotes Cage–Key association and induces the reconstitution of β-lactamase activity. The resulting enzyme

activity was monitored by tracking the absorbance of the nitrocefin hydrolysis product at 490 nm.

Experimental results showed that increasing concentrations of cTnI led to accelerated rates of nitrocefin hydrolysis (Figure 3B), confirming the dose-dependent reconstitution of β-lactamase activity with a 351% activity change, an EC_{50} of 126 nM, and a 75 nM LOD (Figure 3C). Within the linear regime, the solution color shifted visibly from yellow to red within 15 min. As colorimetric readouts are generally less sensitive than optical-based readouts employed previously, the current detection limit does not yet reach the clinically relevant thresholds for AMI diagnosis, which lie in the low-picomolar range.[33] In addition, nitrocefin can undergo spontaneous degradation in serum and generate matrix-derived background signal, so additional serum removal steps may be needed to mitigate interference when used in blood/serum. The sensitivity of our thermodynamic biosensor is limited by the affinity between the recognition module and the target, highlighting the need for higher-affinity recognition elements. Recent advances in computational binder design might provide a promising avenue for the engineering of higher-affinity cTnI binders.[34,35] Incorporating such design strategy into the LOCKR scaffold could enhance sensitivity, bringing colorimetric detection closer to clinically actionable thresholds. Together, these findings demonstrate the adaptability of the LOCKR biosensor platform for colorimetric detection via β-lactamase and highlight its potential for rapid, low-cost, and instrument-free detection.

Expanding Target Analytes for Glucagon, Neuropeptide Y, and Peptide YY

In addition to reprogramming the reporter modules, the modularity of the LOCKR platform can enable quick adaptation to detect new analytes by replacing the recognition domain on the Latch (Figure 4A). To demonstrate this, we incorporated the recent *de novo* picomolar-affinity binders[34] for glucagon (GCG), neuropeptide Y (NPY), and peptide YY (PYY) into the LOCKR platform. These targets are clinically relevant biomarkers for conditions such as hypoglycemia,[36] acute ischemia,[37] inflammatory bowel disease,[38] or other metabolic syndromes. Since these diseases can have a rapid onset and can be life-threatening if not treated promptly, quick detection for these peptide hormones has the potential to improve patient outcomes.

Since the sensing equilibrium is thermodynamically coupled by Cage–Key–Target, the Cage initially forms intramolecular interactions with the binder that prevent Cage–Key association (ΔG_{CK}), holding the switch in the OFF state ($\Delta G_{open} - \Delta G_{CK} > 0$). Upon target peptide binding, the peptide engages and stabilizes the binder in its lowest-energy fold (large ΔG_{BT} due to high-affinity binding), shifting the equilibrium away from the intramolecular Cage–binder interactions that block the Key to facilitate the formation of the Cage–Key complex ($\Delta G_{open} - \Delta G_{CK} - \Delta G_{BT} << 0$), thereby switching the system to the ON state and enabling luciferase reconstitution. To build these new LOCKR biosensors, we used Rosetta GraftSwitch and FastRelax movers to computationally graft the GCG, NPY, and PYY helical binders into the Latch domain of the split-luciferase-based lucCage scaffold,[21] by evaluating axial offsets, junction strains, clashes, and interface packing to identify suitable insertion sites (sampling ΔG_{open}). For each binder, we picked models

visually based on the resulting computational models and experimentally tested nine variants for each target. We subsequently identified functional GCG, NPY, and PYY biosensors that responded to the respective targets (Figure S1). The performance of these two-component and thermodynamically coupled LOCKR biosensors is tunable by varying the Cage–Key stoichiometry without changing the protein sequences (Figure S2). The best-performing GCG biosensor (lucCageGCG2_326, Figure 4B) showed an 846% luminescence increase at saturating glucagon concentrations with a LOD of 168 pM, while the sensitivity of the same biosensor could be tuned to a LOD of 43 pM by adjusting the Cage:Key ratio to 10:50 nM (Figure S2A). The top NPY biosensor (lucCageNPY2_334, Figure 4C) showed a 1225% luminescence response with a 60 pM LOD for neuropeptide Y, and the top PYY biosensor (lucCagePYY4_334, Figure 4D) exhibited a 3623% signal increase with a 23 pM LOD in the presence of peptide YY. Compared to typical physiological concentration ranges, glucagon levels are at ~20–40 pM during hypoglycemia,[39] neuropeptide Y levels are at ~40–60 pM in acute myocardial ischemia,[40] and peptide YY levels are at ~10–20 pM in obese and lean fasting patients.[41] Overall, our GCG, NPY, and PYY biosensors exhibit sensitivities near clinically relevant concentrations under ideal assay conditions. In the presence of human serum (Figure 4, right panels), the biosensor proteins showed reduced fold-of-changes and increased LODs, suggesting that removing serum components may be required for reliable detection at such low concentrations. These results are consistent with prior reports,[6,21,22] in which NanoBiT-based assays are sensitive to assay environment and matrix effects, including variability between individual serum samples. We further showed time-course kinetics for lucCageGCG2_326 to demonstrate the signal onset and reversible switching behavior (Figure 5), similar to the cases that we previously reported.[21,22] Collectively, these results highlight the modularity and tunability of the LOCKR biosensor framework and its compatibility with modern computational binder design to enable the conversion of synthetic binders into functional biosensors.

Engineering Ratiometric Peptide Hormone Biosensors via Intermolecular BRET

With picomolar sensitivity GCG, NPY, and PYY biosensors in hand, we next converted their output to a ratiometric format using an intermolecular BRET configuration. Unlike the above-mentioned intramolecular BRET format, here, we repositioned the fluorescent partner onto the Key protein to enable BRET between two separate protein chains. Specifically, we fused the recently commercialized *de novo* luciferase (LuxSit Pro)[42] as a BRET donor to the N-terminus of the Cage and CyOFP to the C-terminus of the Key (Figure 6A). Upon binding to the target, the thermodynamic equilibrium shifts the Cage protein toward the open state, resulting in Cage–Key association. This brings LuxSit Pro and CyOFP into close proximity, thereby increasing BRET efficiency. Of the six intermolecular BRET biosensors constructed for GCG, NPY, and PYY, three exhibited analyte-dependent changes in BRET efficiency. Across an NPY titration series for luxPro_lucCageNPY2_330, we observed a dose-dependent increase in the emission ratio at 620 nm relative to 508 nm (Figure 6B). At saturated NPY concentrations, the biosensor exhibited a 65% ratiometric change and a 66 nM LOD. For PYY BRET biosensors, luxPro_lucCagePYY4_334 exhibited a 206% ratiometric change and an LOD of 67 nM (Figure 6C), whereas luxPro_lucCagePYY3_344 showed a 138% ratiometric change and an LOD of 71 nM (Figure 6D). These results are consistent with the prior report[43] that ratiometric biosensors often exhibit reduced dynamic

range and sensitivity relative to single-channel intensiometric biosensors. While ratiometric readouts can help mitigate matrix effects, these biosensors function in human serum with a dynamic range and LODs that are comparable to, or slightly better than, those measured in buffer (Figure 6, right panels). Although the ratiometric configuration exhibits slower kinetics toward equilibrium, measurements at 15 min still provide sufficient signal above the baseline for quantification (Figure 7). The sequential addition of the PYY binder as a competitor further suppressed the ratiometric signal, but not completely, indicating that a higher-affinity binder is required to provide sufficient thermodynamic driving force to fully reverse the readout. Overall, these results illustrate that the conformational switching mechanism of the LOCKR switching platform can be adapted to intermolecular BRET output.

CONCLUSIONS

Converting target binding into a reliable signal remains the central challenge in protein-based biosensor design. The LOCKR platform offers a versatile architecture that couples target recognition to signal generation through thermodynamic equilibrium. This modular framework (i) allows rapid retargeting to new analytes by swapping the recognition domain and (ii) enables flexible reconfiguration of the signal output, as demonstrated here through three distinct readout formats: intramolecular BRET, β-lactamase colorimetry, and intermolecular BRET. In parallel, recent advances in computational binder design now make it feasible to generate high-affinity protein binders against targets that previously lacked suitable recognition elements,[44–46] while *de novo* optical reporters also offer more stable light-emitting enzymes for robust outputs.[15,47] Together with other *de novo* switching systems[48–50] beyond LOCKR, these *de novo* components are beginning to bridge the historical gap between binding and transduction, enabling the modular construction of biosensors that convert molecular recognition events into quantitative enzymatic or optical signals. Looking ahead, we anticipate that *de novo*/AI-guided computational protein design[51–56] will continue to accelerate the generation of first-pass biosensor prototypes with desirable target specificity and flexible output compatibility.

Our integrated design-build-test workflow paves the way for modular biosensor design, particularly for targets and settings where natural protein reengineering remains insufficient. However, biosensor performance is often context-dependent with respect to input module affinity and output module responsiveness, which may require additional optimization to meet application-specific requirements. Two-component systems, such as LOCKR, allow flexible tuning by changing stoichiometry and require only a single binder for target recognition, but demand more precise control of assay conditions to ensure consistent performance. Recently, Huang et al. demonstrated the detection of Fumonisin B_1 small molecule using the lucCage-lucKey system,[57] suggesting that the same framework could be potentially reprogrammed to recognize a wider range of analytes or cellular inputs (e.g., tumor antigens or virus markers). As our results expand the design options for repurposing the LOCKR platform, the output modules could be swapped to trigger other biologically relevant enzymatic activities (e.g., kinases[58] or proteases[59]) or other imaging reporters (e.g., reductases[60] or thymidine kinases[61]), enabling the development of a broader class of synthetic biology components in the future.

EXPERIMENTAL SECTION

Materials and General Methods

Synthetic genes were purchased from Integrated DNA Technologies (IDT) as eBlocks. Enzymes including BsaI-HFv2 restriction endonuclease, Q5 PCR polymerase, T5 exonuclease, Phusion DNA polymerase, Taq DNA ligase, and T4 DNA ligase were purchased from New England Biolabs (NEB). Plasmid DNA, PCR products, and digested fragments were purified using Sydlab spin columns, and DNA sequences were verified by Azenta sequencing services. The coelenterazine (CTZ) substrate for the luminescence assay was ordered from GoldBio. Nitrocefin for the colorimetric assay was purchased from Calbiochem. All LuxSit Pro reagents were acquired from the LuxSit Pro Luciferase Assay System (LS0101). Luxterazine stock solution (5 mM) for LuxSit Pro was stored at −80 °C. Human pooled serum was purchased from Fisher Bioreagents. All other chemicals were purchased from Fisher Scientific, Thermo Scientific, or VWR and used as received without further purification. DNA and protein concentrations were measured using a Take3 plate with a Biotek Synergy H1 Plate Reader. Size exclusion chromatography was performed using an ÄKTA pure M system with UNICORN 7 Workstation control (GE Healthcare) coupled with a Superdex 200 Increase 10/300 GL column. Split luciferase and ratiometric BRET assays were carried out in white 96-well microplates (Corning 3921). Colorimetric assays were carried out in clear 96-well microplates (Corning 9017). All luminescence and absorbance measurements were obtained using a Biotek Synergy H1 Plate Reader, with or without specified filters.

General Procedures for Protein Production and Purification

E. coli BL21 (DE3) cells transformed with modified pET29b plasmids containing the gene of interest were grown at 37 °C with shaking at 250 rpm overnight in LB medium supplemented with kanamycin. In the next day, cells were 30-fold diluted in 60 mL of fresh TB medium supplemented with kanamycin and were grown at 37 °C until OD_{600} reached 0.6–0.8. Cells were then induced with 0.5 mM of IPTG at 37 °C for 1 h and then grown at 25 °C overnight. Later, cells were harvested by centrifugation at 4000 g for 20 min and resuspended in 20 mL of lysis buffer (20 mM Tris-HCl pH 8.0, 300 mM NaCl, 30 mM imidazole, and Pierce Protease Inhibitor Tablets). Sonication (10 s and pause for 10 s per cycle; nine cycles) was carried out to lyse the cells followed by high-speed centrifugation at 15,000 g at 12 °C for 45 min to separate the cell debris and soluble proteins. Supernatant containing target proteins was collected and incubated with 600 μL of Ni-NTA nickel agarose beads at 4 °C for 30 min. The beads were transferred into a gravity flow column and washed twice with 10 mL of wash buffer (20 mM Tris-HCl pH 8.0, 300 mM NaCl, 30 mM imidazole) followed by additional serial wash steps: 600 μL of 95:5, then 600 μL of 90:10 (wash:elution buffer), and eluted with 1.2 mL of elution buffer (20 mM Tris-HCl pH 8.0, 300 mM NaCl, 300 mM imidazole). The eluted proteins were purified by size exclusion chromatography in 20 mM Tris-HCl 300 mM NaCl pH 8.0 buffer. Protein concentrations were quantified by NanoDrop OD280, snap-frozen in liquid nitrogen, and stored at −80 °C.

In Vitro Colorimetric Assays

For the colorimetric cTnI biosensor, a premixture was made with 25 μL of 40 nM LacA_lucCageTrop, 25 μL of 40 nM MBP_Key_LacB, and 10 μL of a 2x serially diluted troponin I (GenScript, Z03320). After 15 min of incubation at room temperature, 40 μL of 100 μM nitrocefin was added, resulting in a total of 100 μL in each well with a final concentration of 10 nM LacA_lucCageTrop, 10 nM MBP_Key_LacB, 40 μM nitrocefin, and a 2x serially diluted troponin I (starting from 500 nM). All proteins, analytes, and substrates were prepared in DPBS with calcium (Corning 21–030-CM). Immediately after adding nitrocefin, absorbance at 490 nm was measured using the Synergy H1 Plate Reader every 1 min for a total of 25 min. The initial rate of reconstituted β-lactamase was determined by calculating the slope of the first 5 min and was used for plotting dose–response curves and determining the limit of detection (LOD).

Computational Design of GCG, NPY, and PYY Biosensors

The computational sampling was conducted as previously described.[21] In brief, *de novo* binder sequences that act as the target recognition domain were grafted using RosettaScripts GraftSwitchMover into the α-helical registers between residues 325 and 359 of lucCage. The resulting models were energy-minimized using Rosetta FastRelax to exclude unrealistic strained or clashing configurations guided by the Rosetta score function. All output models (~20 per threaded sequence) were visually inspected with PyMOL by aligning the full-length binder onto the latch. In the cases in which the desired sequence to be inserted exceeded the length of the lucCage latch, we used Rosetta Remodel to model the C-terminus extension of the Cage protein. Constructs were chosen based on the minimal steric hindrance from side chains between the binder and Cage domains. After the removal of redundancies, nine constructs for detecting GCG, NPY, and PYY were selected for subsequent cloning, protein production, and biochemical characterization.

In Vitro Split Luciferase Assays

All computationally designed GCG, NPY, and PYY biosensor constructs were subjected to a preliminary screening assay in the presence of 8 or 0 μM of their respective analyte to narrow down the top candidates for further characterization. For characterization of the split luciferase-based glucagon (lucCageGCG2_326 and lucCageGCG2_330), neuropeptide Y (lucCageNPY2_334 and lucCageNPY2_330), and peptide YY (lucCagePYY4_334 and lucCagePYY3_344) biosensors, a premixture was made with 50 μL of 1x HBS, 10 μL of 500 nM lucCage, 10 μL of 100 nM lucKey, and titrated with 10 μL of their respective analyte (2-fold serial dilution, starting from 50 or 100 μM). After a 15 min incubation at room temperature, 20 μL of 125 μM CTZ was added, resulting in a total of 100 μL in each well with a final concentration of 50 nM lucCage, 10 nM lucKey, 25 μM CTZ, and a 2x serially diluted analyte starting from 5 or 10 μM. Immediately after adding CTZ, luminescence signals were read using the Synergy H1 Plate Reader (Figure S3). The signal was recorded every 1 min for a total of 30 min (integration time = 0.1 s; read mode = kinetic; optic type = luminescence fiber; gain = 120). The highest luminescence RLU value of each triplicate was averaged and used to plot the dose–response curves and LOD graphs. For assays in human serum, premixture containing 40 μL of 1x HBS, 10 μL

of human serum, 10 μL of 500 nM lucCage (lucCageGCG2_326, lucCageNPY2_334, or lucCagePYY4_334), and 10 μL of 100 nM lucKey was made followed by addition of 10 μL of analytes (2x serial dilutions starting from 100 μM). After 15 min of incubation at room temperature, 20 μL of 125 μM CTZ was added, yielding a total volume of 100 μL per well with final concentrations of 50 nM lucCage, 10 nM lucKey, 25 μM CTZ, and a 2x serially diluted analyte starting from 10 μM in HBS buffer. Luminescence measurements were performed as described above.

The reversibility experiment for the lucCageGCG2_326 biosensor was carried out using a mixture of 50 μL of 1x HBS, 10 μL of 100 nM lucCageGCG2_326, and 10 μL of 20 nM lucKey. After the addition of 20 μL of 125 μM CTZ, luminescence was recorded every 30 s for 5 min, followed by the addition of 5 μL of 4 μM GCG analyte. Luminescence was then recorded for another 10 min until the signal stabilized. The GCG analyte was depleted by adding 5 μL of 200 μM GCG binder, and luminescence recording was continued for the remaining 20 min.

In Vitro Ratiometric BRET Assays

For characterizing the intramolecular BRET HBV antibody biosensor, the premixture was made with 25 μL of 40 nM B0622_d6, 25 μL of 80 nM MBP_Key protein, 10 μL of serially diluted HBV antibody HzKR127–3.2, and 30 μL of Cytiva HBS (HEPES-buffered saline)-EP buffer. After a 15 min incubation at room temperature, 10 μL of 50 μM CTZ was added followed by luminescence reading under spectral scanning mode from 350 to 750 nm with 4 nm step intervals. To evaluate the ratiometric change, 460/590 nm ratios were calculated by dividing the average of the three closest values of 460 nm by 590 nm. The LOD was calculated based on plotting the 460/590 nm ratios in triplicate against various HBV antibody concentrations within the linear range. To evaluate baseline BRET efficiency, B0622, B0622_d4, and B0622_d6 were assayed at 10 nM Cage with or without excess MBP_Key protein (10 μM) in the absence of the HBV antibody.

For characterization of the intermolecular BRET NPY and PYY biosensors, the premixture was made with 50 μL of HBS-EP buffer, 10 μL of 500 nM luxPro_lucCage (NPY2_330, PYY4_334, and PYY3_344), and 10 μL of 500 nM Key_CyOFP and titrated with 10 μL of the corresponding analyte in a 2x serial dilution. After 15 min of incubation at room temperature, 20 μL of 125 μM Luxterazine substrate was added, resulting in a total of 100 μL in each well with a final concentration of 50 nM luxPro_lucCage, 50 nM Key_CyOFP, 25 μM substrate, and a 2x serially diluted analyte (starting from 10 μM). All proteins, analytes, and substrates were prepared in 1x HBS. Immediately after adding the substrate, measurements were recorded under spectral scanning mode from 400 to 700 nm with 4 nm step intervals to record the emission spectrum change at different analyte concentrations. The luminescence signal under both 508/20 and 620/40 nm channels was also recorded every 1 min for a total of 15 min in triplicate (integration time = 0.1 s, read mode = kinetic, optic type = filter switching, and gain = 120). The highest RLU values from both the 508 and 620 channels in triplicate were used to calculate 620/508 ratios for plotting the dose–response curves and determining LODs. For assays in human serum, a premixture containing 40 μL of 1x HBS, 10 μL of human serum, 10 μL of 500 nM

luxPro_lucCage, and 10 μL of 500 nM Key_CyOFP was made followed by addition of 10 μL of analytes (2x serial dilutions starting from 100 μM). After 15 min of incubation at room temperature, 20 μL of 125 μM Luxterazine substrate was added, yielding a total volume of 100 μL per well with final concentrations of 50 nM lucCage, 50 nM Key_CyOFP, 25 μM Luxterazine substrate, and a 2x serially diluted analyte starting from 10 μM in HBS buffer. Luminescence measurements were performed as described above.

The reversibility experiment for the intermolecular BRET luxPro_lucCagePYY4_334 biosensor was performed using a mixture containing 50 μL of 1x HBS supplemented with 0.1% BSA and 35 mM thiourea, 10 μL of 50 nM luxPro_lucCagePYY4_334, and 10 μL of 100 nM Key_CyOFP in the same buffer. After the addition of 20 μL of 125 μM Luxterazine substrate in 1x HBS, luminescence was recorded every 1 min for 5 min using 508/20 and 620/40 nm emission filters. Subsequently, 5 μL of indicated PYY concentrations in HBS was added and luminescence was recorded for an additional 45 min. To sequester the PYY analyte, 5 μL of 40 μM PYY binder in HBS was added, and luminescence recording was continued for another 50 min.

Data Processing and Analysis for *in Vitro* Assays

To determine the dynamic range and EC_{50}, assays were carried out under the conditions mentioned above. Intensiometric, ratiometric luminescence signals, and lactamase activity were plotted versus different analyte concentrations. Signals with no analyte were subtracted from the highest signals ($\Delta I = I_{max} - I_{min}$) and divided by the no-analyte signals ($\Delta I / I_{min}$) to determine the dynamic range (DR%). EC_{50} was calculated by fitting the plot to the dose–response stimulation ([Agonist] vs response, variable slope) in Prism 10. For the determination of LOD, reactions with the conditions mentioned above were carried out at the low end of analyte concentrations in technical triplicates. Signal versus different analyte concentrations were plotted and fitted with a linear regression curve in Prism 10 to calculate the slope. LOD was calculated as $3 \times S.D._{y.x}$/slope, where $S.D._{y.x}$ is the standard error of the regression calculated by using the STEYX equation in Excel and the slope is obtained from the linear regression of the data points within the linear response range.

Supplementary Material

Refer to Web version on PubMed Central for supplementary material.

Funding

This research was partially supported by the startup funding from UCSC (C.X. and A.H.-W.Y.) and the NIH NIBIB award R00EB031913 (J.W., J.Y.-H.C., E.A.O., and A.H.-W.Y.).

ABBREVIATIONS

LOCKR	Latching Orthogonal Cage–Key pRotein
FRET	Förster resonance energy transfer
HBV	hepatitis B virus

cTnI	troponin I
GCG	glucagon
NPY	neuropeptide Y
PYY	peptide YY

REFERENCES

(1). Gest AMM; Sahan AZ; Zhong Y; Lin W; Mehta S; Zhang J Molecular Spies in Action: Genetically Encoded Fluorescent Biosensors Light up Cellular Signals. Chem. Rev 2024, 124 (22), 12573–12660. [PubMed: 39535501]

(2). Zhang Y; Looger LL Fast and Sensitive GCaMP Calcium Indicators for Neuronal Imaging. J. Physiol 2024, 602 (8), 1595–1604. [PubMed: 36811153]

(3). Yeh H-W; Ai H-W Development and Applications of Bioluminescent and Chemiluminescent Reporters and Biosensors. Annu. Rev. Anal. Chem 2019, 12 (1), 129–150.

(4). Adamson H; Ajayi MO; Campbell E; Brachi E; Tiede C; Tang AA; Adams TL; Ford R; Davidson A; Johnson M; McPherson MJ; Tomlinson DC; Jeuken LJC Affimer–Enzyme–Inhibitor Switch Sensor for Rapid Wash-Free Assays of Multimeric Proteins. ACS Sens 2019, 4 (11), 3014–3022. [PubMed: 31578863]

(5). Hellweg L; Edenhofer A; Barck L; Huppertz M-C; Frei MS; Tarnawski M; Bergner A; Koch B; Johnsson K; Hiblot J A General Method for the Development of Multicolor Biosensors with Large Dynamic Ranges. Nat. Chem. Biol 2023, 19 (9), 1147–1157. [PubMed: 37291200]

(6). Ni Y; Rosier BJHM; van Aalen EA; Hanckmann ETL; Biewenga L; Pistikou A-MM; Timmermans B; Vu C; Roos S; Arts R; Li W; de Greef TFA; van Borren MMGJ; van Kuppeveld FJM; Bosch B-J; Merkx M A Plug-and-Play Platform of Ratiometric Bioluminescent Sensors for Homogeneous Immunoassays. Nat. Commun 2021, 12 (1), No. 4586. [PubMed: 34321486]

(7). Yu Q; Xue L; Hiblot J; Griss R; Fabritz S; Roux C; Binz P-A; Haas D; Okun JG; Johnsson K Semisynthetic Sensor Proteins Enable Metabolic Assays at the Point of Care. Science 2018, 361 (6407), 1122–1126. [PubMed: 30213915]

(8). Hiblot J; Yu Q; Sabbadini MDB; Reymond L; Xue L; Schena A; Sallin O; Hill N; Griss R; Johnsson K Luciferases with Tunable Emission Wavelengths. Angew. Chem., Int. Ed 2017, 56 (46), 14556–14560.

(9). Fox DR; Taveneau C; Clement J; Grinter R; Knott GJ Code to Complex: AI-Driven de Novo Binder Design. Structure 2025, 33 (10), 1631–1642. [PubMed: 40897171]

(10). Yang W; Wang S; Lee GR; Zhang JZ; Courbet A; Juergens D; Wang X; Schlichthaerle T; Abedi M; Ragotte R; An L; Kalvet I; Pellock S; Mihaljevic L; Glasscock C; Pillai A; Broerman A; Ennist N; Haefner E; McNamara-Bordewick N; Haydon I; Stewart L; Bhardwaj G; Baker D The Past, Present and Future of de Novo Protein Design. Nature 2026, 652 (8112), 1139–1152. [PubMed: 42056544]

(11). Cao L; Coventry B; Goreshnik I; Huang B; Sheffler W; Park JS; Jude KM; Marković I; Kadam RU; Verschueren KHG; Verstraete K; Walsh STR; Bennett N; Phal A; Yang A; Kozodoy L; DeWitt M; Picton L; Miller L; Strauch E-M; DeBouver ND; Pires A; Bera AK; Halabiya S; Hammerson B; Yang W; Bernard S; Stewart L; Wilson IA; Ruohola-Baker H; Schlessinger J; Lee S; Savvides SN; Garcia KC; Baker D Design of Protein-Binding Proteins from the Target Structure Alone. Nature 2022, 605 (7910), 551–560. [PubMed: 35332283]

(12). Bennett NR; Coventry B; Goreshnik I; Huang B; Allen A; Vafeados D; Peng YP; Dauparas J; Baek M; Stewart L; DiMaio F; De Munck S; Savvides SN; Baker D Improving de Novo Protein Binder Design with Deep Learning. Nat. Commun 2023, 14 (1), No. 2625. [PubMed: 37149653]

(13). Bennett NR; Watson JL; Ragotte RJ; Borst AJ; See DL; Weidle C; Biswas R; Yu Y; Shrock EL; Ault R; Leung PJY; Huang B; Goreshnik I; Tam J; Carr KD; Singer B; Criswell C; Wicky BIM; Vafeados D; Garcia Sanchez M; Kim HM; Vázquez Torres S; Chan S; Sun SM; Spear TT; Sun Y; O'Reilly K; Maris JM; Sgourakis NG; Melnyk RA; Liu CC; Baker D Atomically Accurate

de Novo Design of Antibodies with RFdiffusion. Nature 2026, 649 (8095), 183–193. [PubMed: 41193805]

(14). Dou JY; Vorobieva AA; Sheffler W; Doyle LA; Park H; Bick MJ; Mao BC; Foight GW; Lee MY; Gagnon LA; Carter L; Sankaran B; Ovchinnikov S; Marcos E; Huang PS; Vaughan JC; Stoddard BL; Baker D De Novo Design of a Fluorescence-Activating Beta-Barrel. Nature 2018, 561 (7724), 485–491. [PubMed: 30209393]

(15). Yeh AH-W; Norn C; Kipnis Y; Tischer D; Pellock SJ; Evans D; Ma P; Lee GR; Zhang JZ; Anishchenko I; Coventry B; Cao L; Dauparas J; Halabiya S; DeWitt M; Carter L; Houk KN; Baker D De Novo Design of Luciferases Using Deep Learning. Nature 2023, 614 (7949), 774–780. [PubMed: 36813896]

(16). Kortemme T De Novo Protein Design—From New Structures to Programmable Functions. Cell 2024, 187 (3), 526–544. [PubMed: 38306980]

(17). Langan RA; Boyken SE; Ng AH; Samson JA; Dods G; Westbrook AM; Nguyen TH; Lajoie MJ; Chen Z; Berger S; Mulligan VK; Dueber JE; Novak WRP; El-Samad H; Baker D De Novo Design of Bioactive Protein Switches. Nature 2019, 572 (7768), 205–210. [PubMed: 31341284]

(18). Lajoie MJ; Boyken SE; Salter AI; Bruffey J; Rajan A; Langan RA; Olshefsky A; Muhunthan V; Bick MJ; Gewe M; Quijano-Rubio A; Johnson J; Lenz G; Nguyen A; Pun S; Correnti CE; Riddell SR; Baker D Designed Protein Logic to Target Cells with Precise Combinations of Surface Antigens. Science 2020, 369 (6511), 1637–1643. [PubMed: 32820060]

(19). Zhang JZ; Ong S-E; Baker D; Maly DJ Single-Cell Sensor Analyses Reveal Signaling Programs Enabling Ras-G12C Drug Resistance. Nat. Chem. Biol 2025, 21 (1), 47–58. [PubMed: 39103633]

(20). Zhang JZ; Nguyen WH; Greenwood N; Rose JC; Ong S-E; Maly DJ; Baker D Computationally Designed Sensors Detect Endogenous Ras Activity and Signaling Effectors at Subcellular Resolution. Nat. Biotechnol 2024, 42 (12), 1888–1898. [PubMed: 38273065]

(21). Quijano-Rubio A; Yeh HW; Park J; Lee H; Langan RA; Boyken SE; Lajoie MJ; Cao LX; Chow CM; Miranda MC; Wi J; Hong HJ; Stewart L; Oh BH; Baker D De Novo Design of Modular and Tunable Protein Biosensors. Nature 2021, 591 (7850), 482–487. [PubMed: 33503651]

(22). Zhang JZ; Yeh H-W; Walls AC; Wicky BIM; Sprouse KR; VanBlargan LA; Treger R; Quijano-Rubio A; Pham MN; Kraft JC; Haydon IC; Yang W; DeWitt M; Bowen JE; Chow CM; Carter L; Ravichandran R; Wener MH; Stewart L; Veesler D; Diamond MS; Greninger AL; Koelle DM; Baker D Thermodynamically Coupled Biosensors for Detecting Neutralizing Antibodies against SARS-CoV-2 Variants. Nat. Biotechnol 2022, 40 (9), 1336–1340. [PubMed: 35484405]

(23). Xi C; Yeh AH-W Decoding Luciferase Signal Dynamics: A Roadmap to Reliable Luminescent Assays. JACS Au 2026, 6 (3), 1739–1756.

(24). Ni Y; Arts R; Merkx M Ratiometric Bioluminescent Sensor Proteins Based on Intramolecular Split Luciferase Complementation. ACS Sens 2019, 4 (1), 20–25. [PubMed: 30525479]

(25). van Rosmalen M; Ni Y; Vervoort DFM; Arts R; Ludwig SKJ; Merkx M Dual-Color Bioluminescent Sensor Proteins for Therapeutic Drug Monitoring of Antitumor Antibodies. Anal. Chem 2018, 90 (5), 3592–3599. [PubMed: 29443503]

(26). Engelen W; van de Wiel KM; Meijer LHH; Saha B; Merkx M Nucleic Acid Detection Using BRET-Beacons Based on Bioluminescent Protein–DNA Hybrids. Chem. Commun 2017, 53 (19), 2862–2865.

(27). Arts R; den Hartog I; Zijlema SE; Thijssen V; van der Beelen SHE; Merkx M Detection of Antibodies in Blood Plasma Using Bioluminescent Sensor Proteins and a Smartphone. Anal. Chem 2016, 88 (8), 4525–4532. [PubMed: 27018236]

(28). Yeh H-W; Karmach O; Ji A; Carter D; Martins-Green MM; Ai H-W Red-Shifted Luciferase–Luciferin Pairs for Enhanced Bioluminescence Imaging. Nat. Methods 2017, 14 (10), 971–974. [PubMed: 28869756]

(29). Chu J; Oh Y; Sens A; Ataie N; Dana H; Macklin JJ; Laviv T; Welf ES; Dean KM; Zhang F; Kim BB; Tang CT; Hu M; Baird MA; Davidson MW; Kay MA; Fiolka R; Yasuda R; Kim DS; Ng H-L; Lin MZ A Bright Cyan-Excitable Orange Fluorescent Protein Facilitates Dual-Emission Microscopy and Enhances Bioluminescence Imaging in Vivo. Nat. Biotechnol 2016, 34 (7), 760–767. [PubMed: 27240196]

(30). Kim JH; Gripon P; Bouezzedine F; Jeong MS; Chi S-W; Ryu S-E; Hong HJ Enhanced Humanization and Affinity Maturation of Neutralizing Anti-Hepatitis B Virus PreS1 Antibody Based on Antigen-Antibody Complex Structure. FEBS Lett 2015, 589 (2), 193–200. [PubMed: 25481411]

(31). Tomimuro K; Tenda K; Ni Y; Hiruta Y; Merkx M; Citterio D Thread-Based Bioluminescent Sensor for Detecting Multiple Antibodies in a Single Drop of Whole Blood. ACS Sens 2020, 5 (6), 1786–1794. [PubMed: 32441095]

(32). Galarneau A; Primeau M; Trudeau L-E; Michnick SW Beta-Lactamase Protein Fragment Complementation Assays as in Vivo and in Vitro Sensors of Protein Protein Interactions. Nat. Biotechnol 2002, 20 (6), 619–622. [PubMed: 12042868]

(33). Rubini Gimenez M; Twerenbold R; Jaeger C; Schindler C; Puelacher C; Wildi K; Reichlin T; Haaf P; Merk S; Honegger U; Wagener M; Druey S; Schumacher C; Krivoshei L; Hillinger P; Herrmann T; Campodarve I; Rentsch K; Bassetti S; Osswald S; Mueller C One-Hour Rule-in and Rule-out of Acute Myocardial Infarction Using High-Sensitivity Cardiac Troponin I. Am. J. Med 2015, 128 (8), 861–870.e4. [PubMed: 25840034]

(34). Vázquez Torres S; Leung PJY; Venkatesh P; Lutz ID; Hink F; Huynh H-H; Becker J; Yeh AH-W; Juergens D; Bennett NR; Hoofnagle AN; Huang E; MacCoss MJ; Expòsit M; Lee GR; Bera AK; Kang A; De La Cruz J; Levine PM; Li X; Lamb M; Gerben SR; Murray A; Heine P; Korkmaz EN; Nivala J; Stewart L; Watson JL; Rogers JM; Baker D De Novo Design of High-Affinity Binders of Bioactive Helical Peptides. Nature 2024, 626 (7998), 435–442. [PubMed: 38109936]

(35). Wu K; Jiang H; Hicks DR; Liu C; Muratspahić E; Ramelot TA; Liu Y; McNally K; Kenny S; Mihut A; Gaur A; Coventry B; Chen W; Bera AK; Kang A; Gerben S; Lamb MY-L; Murray A; Li X; Kennedy MA; Yang W; Song Z; Schober G; Brierley SM; O'Neill J; Gelb MH; Montelione GT; Derivery E; Baker D Design of Intrinsically Disordered Region Binding Proteins. Science 2025, 389 (6757), No. eadr8063. [PubMed: 40674483]

(36). Sprague JE; Arbeláez AM Glucose Counterregulatory Responses to Hypoglycemia. Pediatr. Endocrinol. Rev 2011, 9 (1), 463–473. [PubMed: 22783644]

(37). Gibbs T; Tapoulal N; Shanmuganathan M; Burrage MK; Borlotti A; Banning AP; Choudhury RP; Neubauer S; Kharbanda RK; Ferreira VM; Channon KM; Herring N; OxAMI (Oxford Acute Myocardial Infarction) Study, Neuropeptide-Y Levels in ST-Segment-Elevation Myocardial Infarction: Relationship with Coronary Microvascular Function, Heart Failure, and Mortality. J. Am. Heart Assoc 2022, 11 (13), No. e024850. [PubMed: 35766271]

(38). El-Salhy M; Solomon T; Hausken T; Gilja OH; Hatlebakk JG Gastrointestinal Neuroendocrine Peptides/Amines in Inflammatory Bowel Disease. World J. Gastroenterol 2017, 23 (28), 5068–5085. [PubMed: 28811704]

(39). Banarer S; McGregor VP; Cryer PE Intraislet Hyperinsulinemia Prevents the Glucagon Response to Hypoglycemia despite an Intact Autonomic Response. Diabetes 2002, 51 (4), 958–965. [PubMed: 11916913]

(40). Omland T; Opstad PK; Dickstein K Plasma Neuropeptide Y Levels in the Acute and Early Convalescent Phase after Myocardial Infarction. Am. Heart J 1994, 127 (4), 774–779. [PubMed: 8154414]

(41). Batterham RL; Cohen MA; Ellis SM; Le Roux CW; Withers DJ; Frost GS; Ghatei MA; Bloom S R Inhibition of Food Intake in Obese Subjects by Peptide $YY_{3–36}$. N. Engl. J. Med 2003, 349 (10), 941–948. [PubMed: 12954742]

(42). Vergara R; Wagner J; Kamalian P; Harman JL; Lara N; Fischer ES; Bernardes GJL; Quijano-Rubio A; Silva D-A LuxSit Pro and SPro: Next-Generation Designed Luciferases for Bioluminescent Reporting and Complementation-Based Detection. bioRxiv 2025, No. 665742.

(43). Gräwe A; Merkx M Bioluminescence Goes Dark: Boosting the Performance of Bioluminescent Sensor Proteins Using Complementation Inhibitors. ACS Sens 2022, 7 (12), 3800–3808. [PubMed: 36450135]

(44). Liu B; Greenwood NF; Bonzanini JE; Motmaen A; Meyerberg J; Dao T; Xiang X; Ault R; Sharp J; Wang C; Visani GM; Vafeados DK; Roullier N; Nourmohammad A; Scheinberg DA; Garcia KC; Baker D Design of High-Specificity Binders for Peptide-MHC-I Complexes. Science 2025, 389 (6758), 386–391. [PubMed: 40705892]

(45). Liu C; Wu K; Choi H; Han HL; Zhang X; Watson JL; Ahn G; Zhang JZ; Shijo S; Good LL; Fischer CM; Bera AK; Kang A; Brackenbrough E; Coventry B; Hick DR; Qamar S; Li X; Decarreau J; Gerben SR; Yang W; Goreshnik I; Vafeados D; Wang X; Lamb M; Murray A; Kenny S; Bauer MS; Hoofnagle AN; Zhu P; Knowles TPJ; Baker D Diffusing Protein Binders to Intrinsically Disordered Proteins. Nature 2025, 644 (8077), 809–817. [PubMed: 40739343]

(46). Yang W; Hicks DR; Ghosh A; Schwartze TA; Conventry B; Goreshnik I; Allen A; Halabiya SF; Kim CJ; Hinck CS; Lee DS; Bera AK; Li Z; Wang Y; Schlichthaerle T; Cao L; Huang B; Garrett S; Gerben SR; Rettie S; Heine P; Murray A; Edman N; Carter L; Stewart L; Almo SC; Hinck AP; Baker D Design of High-Affinity Binders to Immune Modulating Receptors for Cancer Immunotherapy. Nat. Commun 2025, 16 (1), No. 2001. [PubMed: 40011465]

(47). Chen JY-H; Shi Q; Peng X; de D. Habimana J; Wang J; Sobolewski W; Yeh AH-W De Novo Luciferases Enable Multiplexed Bioluminescence Imaging. Chem 2024, 11 (3), No. 102346. [PubMed: 40417169]

(48). Praetorius F; Leung PJY; Tessmer MH; Broerman A; Demakis C; Dishman AF; Pillai A; Idris A; Juergens D; Dauparas J; Li X; Levine PM; Lamb M; Ballard RK; Gerben SR; Nguyen H; Kang A; Sankaran B; Bera AK; Volkman BF; Nivala J; Stoll S; Baker D Design of Stimulus-Responsive Two-State Hinge Proteins. Science 2023, 381 (6659), 754–760. [PubMed: 37590357]

(49). Chen JY-H; Peng X; Xi C; Lee GR; Baker D; Yeh AH-W De Novo Design of High-Performance Cortisol Luminescent Biosensors. J. Am. Chem. Soc 2025, 147 (31), 27494–27505. [PubMed: 40720516]

(50). Broerman AJ; Pollmann C; Zhao Y; Lichtenstein MA; Jackson MD; Tessmer MH; Ryu WH; Ogishi M; Abedi MH; Sahtoe DD; Allen A; Kang A; De La Cruz J; Brackenbrough E; Sankaran B; Bera AK; Zuckerman DM; Stoll S; Garcia KC; Praetorius F; Piehler J; Baker D Design of Facilitated Dissociation Enables Timing of Cytokine Signalling. Nature 2025, 647, 528–535. [PubMed: 40993395]

(51). Watson JL; Juergens D; Bennett NR; Trippe BL; Yim J; Eisenach HE; Ahern W; Borst AJ; Ragotte RJ; Milles LF; Wicky BIM; Hanikel N; Pellock SJ; Courbet A; Sheffler W; Wang J; Venkatesh P; Sappington I; Torres SV; Lauko A; De Bortoli V; Mathieu E; Ovchinnikov S; Barzilay R; Jaakkola TS; DiMaio F; Baek M; Baker D De Novo Design of Protein Structure and Function with RFdiffusion. Nature 2023, 620 (7976), 1089–1100. [PubMed: 37433327]

(52). Krishna R; Wang J; Ahern W; Sturmfels P; Venkatesh P; Kalvet I; Lee GR; Morey-Burrows FS; Anishchenko I; Humphreys IR; McHugh R; Vafeados D; Li X; Sutherland GA; Hitchcock A; Hunter CN; Kang A; Brackenbrough E; Bera AK; Baek M; DiMaio F; Baker D Generalized Biomolecular Modeling and Design with RoseTTAFold All-Atom. Science 2024, 384 (6693), No. eadl2528. [PubMed: 38452047]

(53). An L; Said M; Tran L; Majumder S; Goreshnik I; Lee GR; Juergens D; Dauparas J; Anishchenko I; Coventry B; Bera AK; Kang A; Levine PM; Alvarez V; Pillai A; Norn C; Feldman D; Zorine D; Hicks DR; Li X; Sanchez MG; Vafeados DK; Salveson PJ; Vorobieva AA; Baker D Binding and Sensing Diverse Small Molecules Using Shape-Complementary Pseudocycles. Science 2024, 385 (6706), 276–282. [PubMed: 39024436]

(54). Dauparas J; Lee GR; Pecoraro R; An L; Anishchenko I; Glasscock C; Baker D Atomic Context-Conditioned Protein Sequence Design Using LigandMPNN. Nat. Methods 2025, 22 (4), 717–723. [PubMed: 40155723]

(55). Lee GR; Pellock SJ; Norn C; Tischer D; Dauparas J; Anishchenko I; Mercer JAM; Kang A; Bera AK; Nguyen H; Brackenbrough E; Sankaran B; Goreshnik I; Vafeados D; Roullier N; Han HL; Coventry B; Haddox HK; Liu DR; Yeh AH-W; Baker D Small-Molecule Binding and Sensing with a Designed Protein Family. Nat. Commun 2026, 17, No. 4533. [PubMed: 41904144]

(56). Ahern W; Yim J; Tischer D; Salike S; Woodbury SM; Kim D; Kalvet I; Kipnis Y; Coventry B; Altae-Tran HR; Bauer MS; Barzilay R; Jaakkola TS; Krishna R; Baker D Atom-Level Enzyme Active Site Scaffolding Using RFdiffusion2. Nat. Methods 2026, 23 (1), 96–105. [PubMed: 41339749]

(57). Huang B; Sun M; Liu X; Cai C; Wei T; Huang M; Tu Z; Li Y; He Q Mimotope-Driven lucCage-LucKey Homogeneous Bioluminescent Immunosensor for the Small Molecule Fumonisin B1. Anal. Chem 2026, 98 (18).

(58). Diaz JE; Morgan CW; Minogue CE; Hebert AS; Coon JJ; Wells JA A Split-Abl Kinase for Direct Activation in Cells. Cell Chem. Biol 2017, 24 (10), 1250–1258. [PubMed: 28919041]

(59). Gray DC; Mahrus S; Wells JA Activation of Specific Apoptotic Caspases with an Engineered Small-Molecule-Activated Protease. Cell 2010, 142 (4), 637–646. [PubMed: 20723762]

(60). Shimojo M; Ono M; Takuwa H; Mimura K; Nagai Y; Fujinaga M; Kikuchi T; Okada M; Seki C; Tokunaga M; Maeda J; Takado Y; Takahashi M; Minamihisamatsu T; Zhang M-R; Tomita Y; Suzuki N; Maximov A; Suhara T; Minamimoto T; Sahara N; Higuchi M A Genetically Targeted Reporter for PET Imaging of Deep Neuronal Circuits in Mammalian Brains. EMBO J 2021, 40 (22), No. e107757. [PubMed: 34636430]

(61). Massoud TF; Paulmurugan R; Gambhir SS A Molecularly Engineered Split Reporter for Imaging Protein-Protein Interactions with Positron Emission Tomography. Nat. Med 2010, 16 (8), 921–926. [PubMed: 20639890]

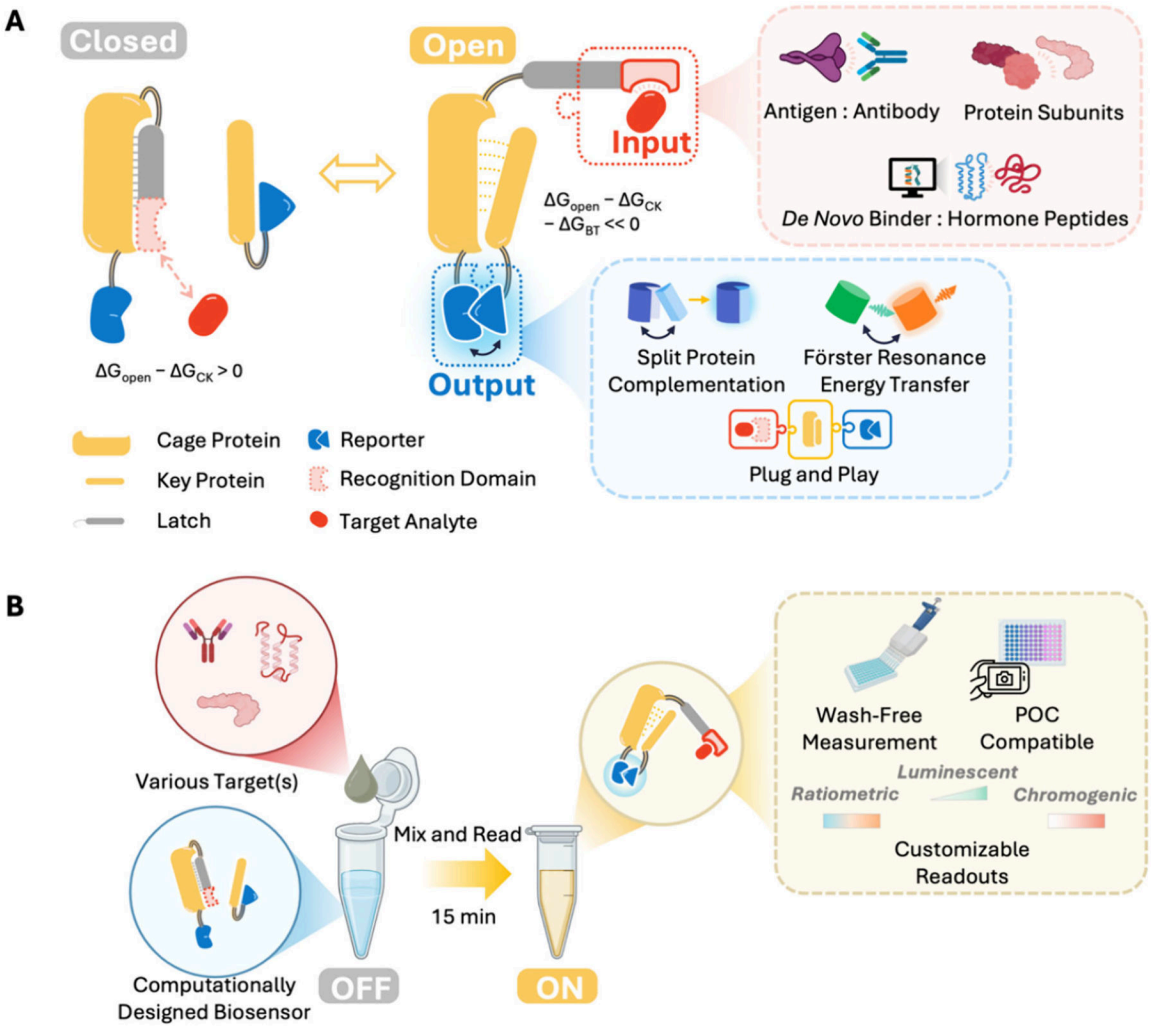

Figure 1.

Overview and features of LOCKR-based biosensor design. The LOCKR system is thermodynamically tuned so that, without target, the binding free energy of Cage and Key (ΔG_{CK}) is insufficient to pay the energetic cost of Cage opening (ΔG_{open}), keeping the switch in the closed state ($\Delta G_{open} - \Delta G_{CK} > 0$). With target present, the binder–target interactions contribute additional binding free energy (ΔG_{BT}), driving equilibrium toward the open state ($\Delta G_{open} - \Delta G_{CK} - \Delta G_{BT} << 0$). (A) Modular architecture: LOCKR is a *de novo* protein switch in which a preorganized helical Cage stabilizes a closed OFF conformation by sequestering a latch that carries the target-binding domain and the inactive split-reporter fragment. The recognition domain on the latch is interchangeable to retarget the biosensor to diverse analyte inputs, and the split reporter can be swapped for alternative output modalities, enabling plug-and-play utilities. (B) Homogeneous assay: LOCKR biosensors support a rapid, mix-and-read workflow in which the output becomes detectable within 15 min in an all-in-solution, homogeneous, and wash-free format. In the absence of analyte, the closed conformation prevents activation; thus, the system stays in the OFF state. Target engagement unlocks the latch, exposes the Cage–Key interface, and shifts the biosensor to the ON state. These computationally designed biosensors are compatible

with a broad range of targets and support customizable outputs, including luminescent (split luciferase), chromogenic (split β-lactamase), and ratiometric Förster-type resonance energy transfer readouts.

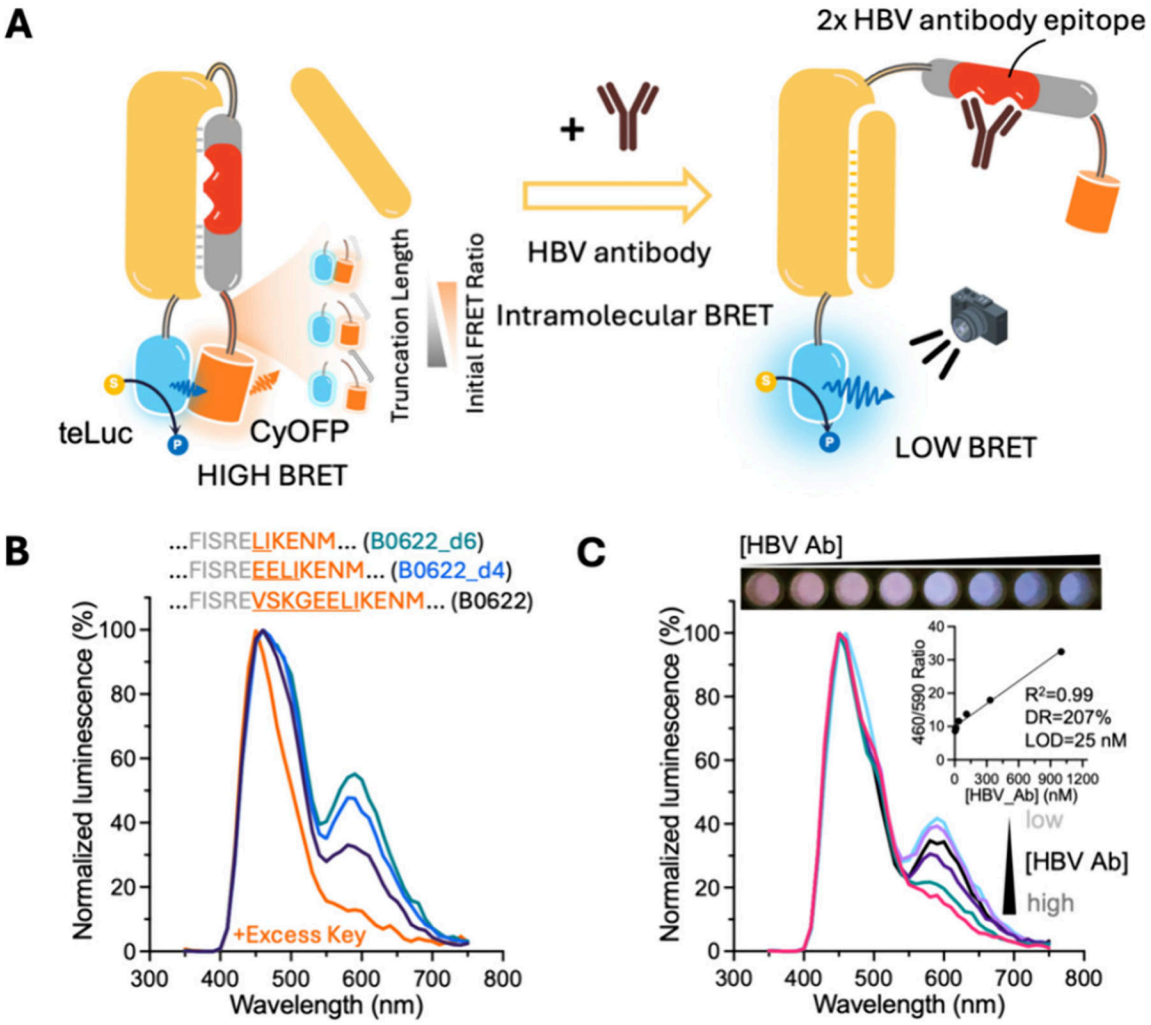

Figure 2.

Design and characterization of the BRET-based HBV antibody biosensor using teLuc-CyOFP proximity. (A) Schematic diagram of the intramolecular BRET HBV antibody biosensor. In the OFF state, the close proximity between the donor (teLuc) and the acceptor (CyOFP) results in high BRET efficiency. Upon antibody binding to the epitope inserted within the latch, the Cage–Latch interaction is disrupted, switching the conformational ensemble toward the open state. This increases the distance between the donor and acceptor, thereby reducing BRET efficiency. (B) The N-terminus of CyOFP was truncated by 0 (B0622), 4 (B0622_d4), or 6 (B0622_d6) residues to assess the initial BRET efficiency. Variants with different truncation lengths were evaluated for baseline BRET efficiency using 10 nM biosensor. B0622_d6 with higher initial BRET ratios yielded an expanded dynamic range upon activation, while excess Key protein switched the Cage protein to the open state (low BRET). (C) HBV antibody titration elicited ratiometric, dose-dependent shifts in the BRET emission spectrum of B0622_d6. The luminescence hue transitioned from reddish to bluish with increased antibody concentrations. The color image was acquired by a smartphone camera. LOD was calculated as 3 × S.D.$_{y.x}$/slope. The assay was performed

in Cytiva HBS-EP (10 mM HEPES, 150 mM NaCl, 3 mM EDTA, and 0.05% v/v Surfactant P20).

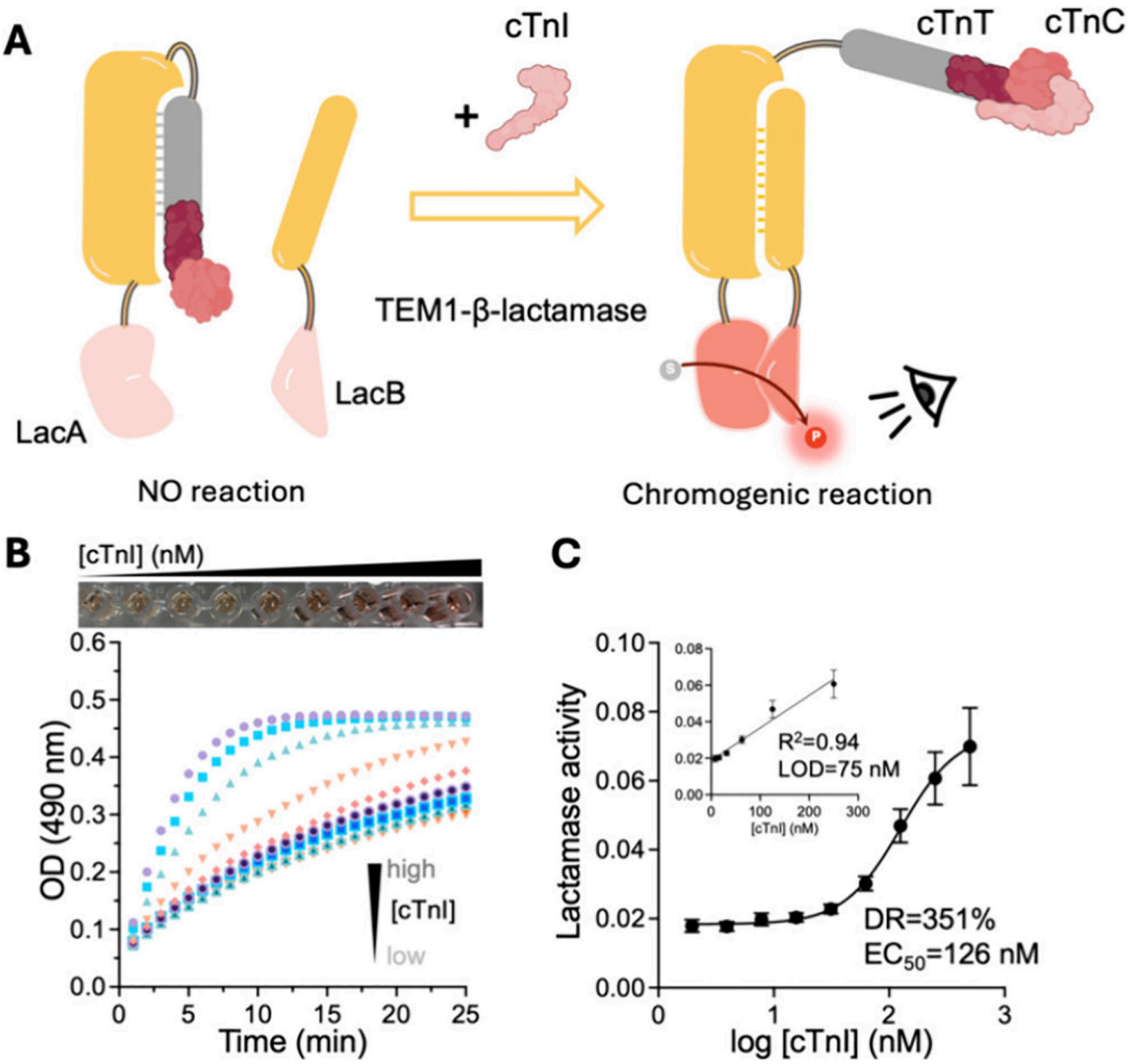

Figure 3.

Design and characterization of human cardiac troponin I (cTnI) colorimetric biosensor using split β-lactamase. (A) Schematic diagram of the colorimetric troponin I biosensor. In the OFF state, the Cage and Key domains remain dissociated, preventing reassembly of split TEM1-β-lactamase (LacA and LacB). Upon cTnI binding to the fused cTnT/cTnC recognition domains on the Latch, the conformational equilibrium shifts to the ON state, promoting Cage–Key association and reconstitution of β-lactamase activity (~10% of intact TEM1 activity). The active enzyme hydrolyzes the chromogenic substrate nitrocefin, resulting in a color change from yellow to red that is visible by eye. (B) Reaction kinetics of nitrocefin hydrolysis using 10 nM LacA_lucCageTrop and 10 nM MBP_Key_LacB in response to varying concentrations of cTnI. The photo above shows the dose-dependent color change in solution from yellow to reddish in the presence of cTnI. (C) Changes of β-lactamase activities in response to various concentrations of cTnI to estimate dynamic range, EC_{50}, and LOD. LOD was calculated as 3 × $S.D._{y.x}$/slope.

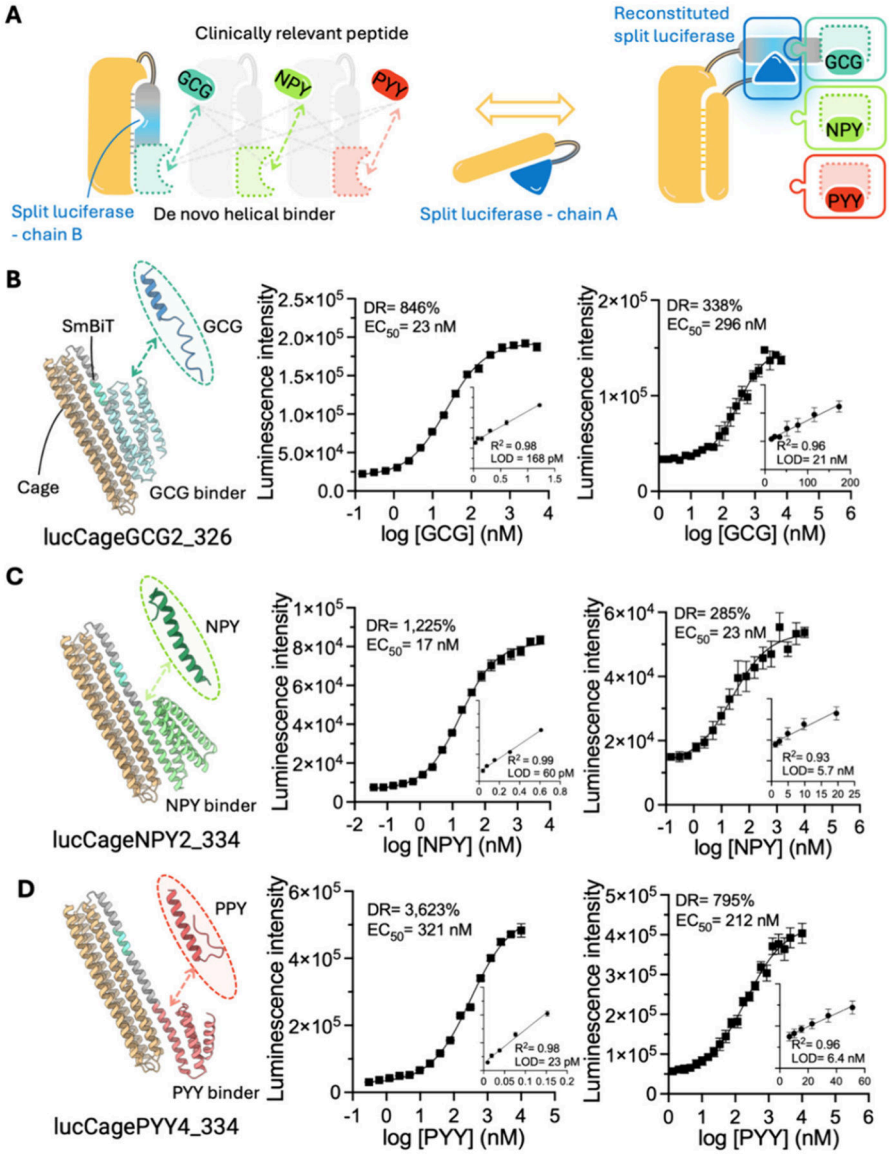

Figure 4.

Design and characterization of glucagon (GCG), neuropeptide Y (NPY), and peptide YY (PYY) biosensors. (A) Swapping the recognition domains with *de novo* designed binders of glucagon, neuropeptide Y, and peptide YY, yielded corresponding luminescent biosensors using split luciferase (LgBiT/SmBiT) as the reporter module. Dose–response curves were used to determine dynamic range, EC_{50}, and LOD for (B) lucCageGCG2_326 to detect GCG, (C) lucCageNPY2_334 to detect NPY, and (D) lucCagePYY4_334 to detect PYY. The design model (left), dose–response curve/LOD in HBS buffer (middle), or 10% human pooled serum (right) is shown. Luminescence assays were performed with 50 nM Cage and 10 nM Key proteins, incubated with serial dilutions of the target analyte. All experiments were performed in triplicate and data represent mean ± s.d. LOD was calculated as 3 × $S.D._{y.x}$/slope.

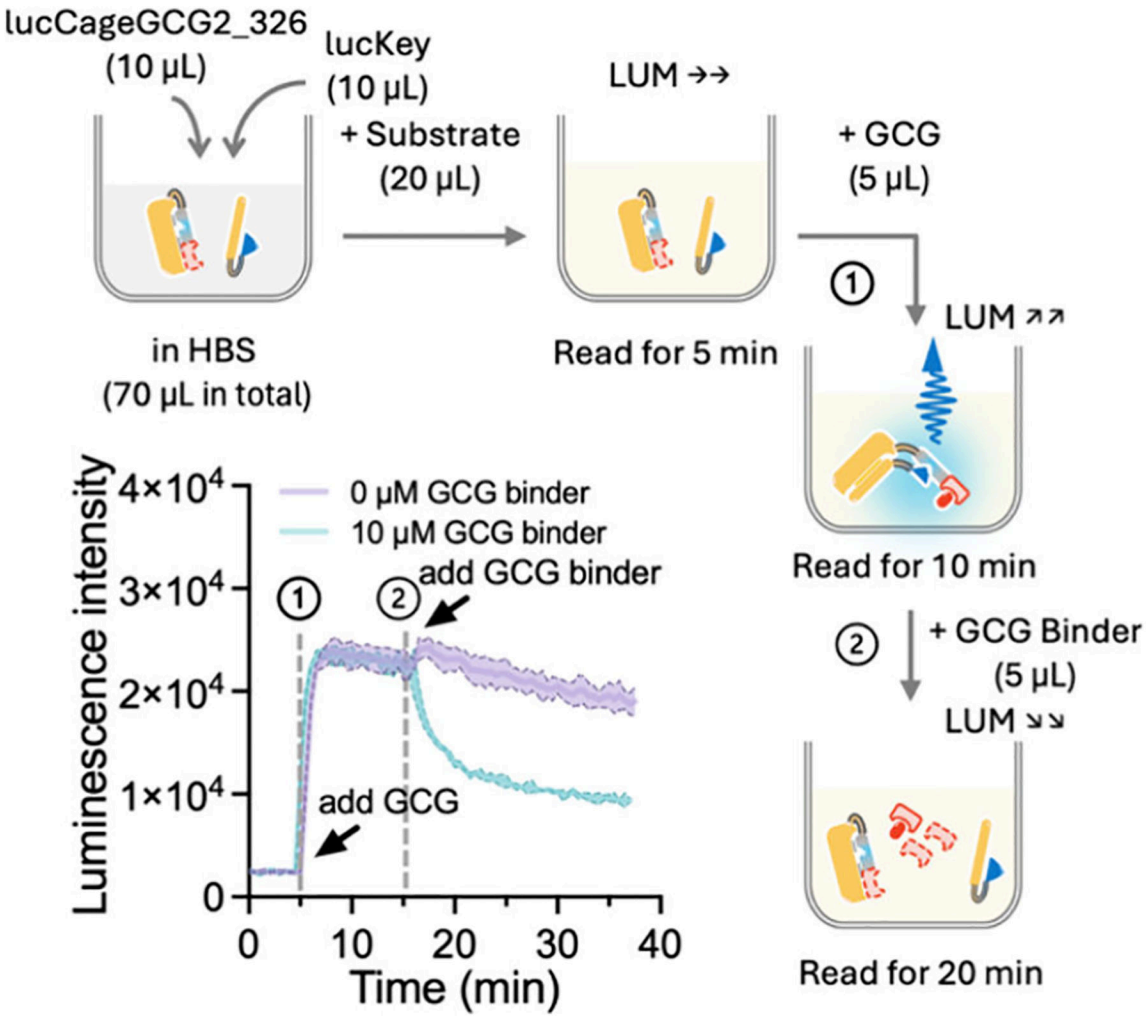

Figure 5.

Luminescence signal kinetics and reversibility of lucCageGCG2_326. lucCageGCG2_326 and lucKey proteins were premixed in HBS buffer with CTZ substrate to establish the baseline luminescence signal. Time-course luminescence traces of lucCageGCG2_326 were then recorded following sequential addition of 200 nM GCG (left arrows) at 5 min, followed by either 0 μM (purple) or 10 μM (green) *de novo* GCG binder (right arrows) at 15 min. Data represent mean ± s.d. from triplicate measurements.

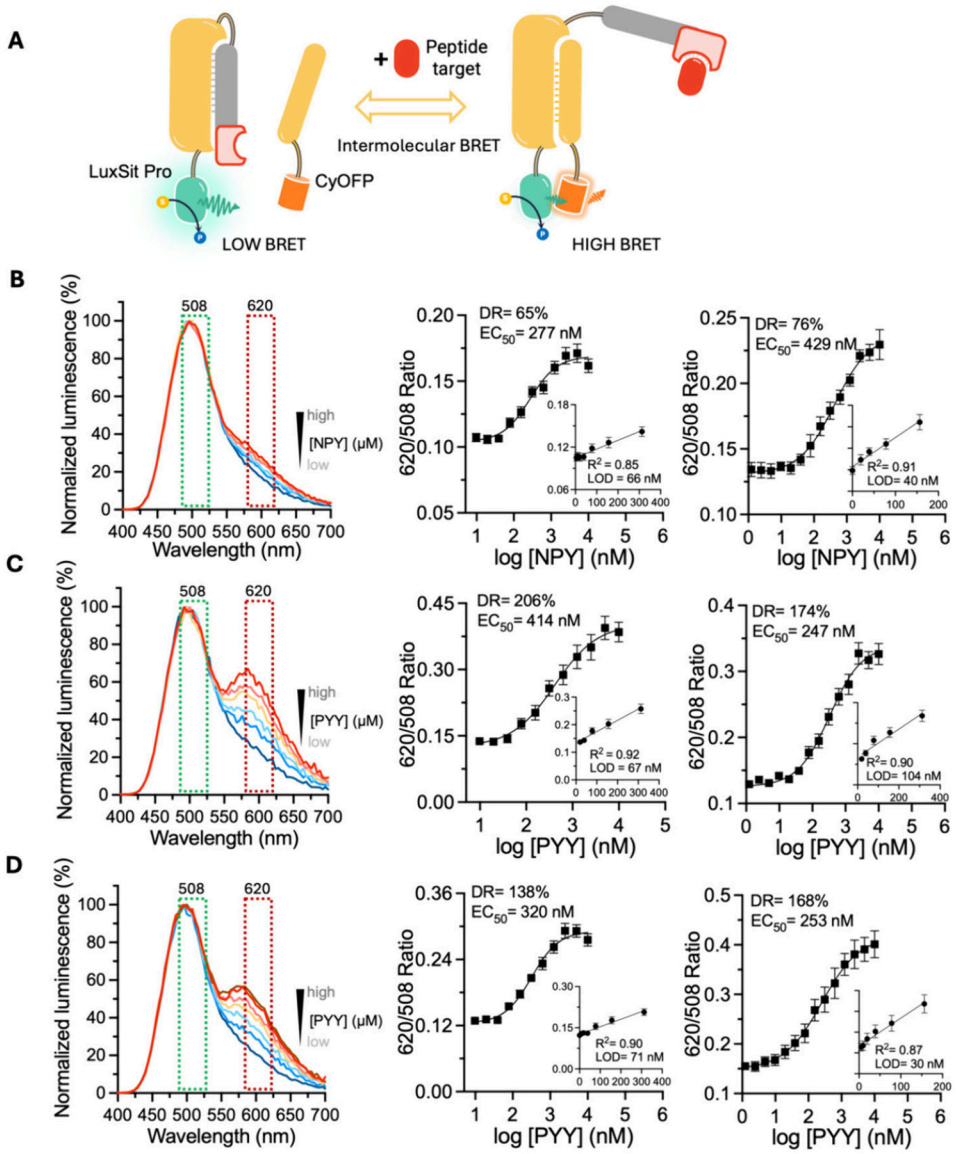

Figure 6.

Design and characterization of intermolecular BRET biosensors for neuropeptide Y (NPY) and peptide YY (PYY). (A) Schematic diagram of the intermolecular BRET biosensor. In the absence of the target, the donor (LuxSit Pro) and the acceptor (CyOFP) are spatially separated, resulting in low BRET efficiency. Upon target binding, the thermodynamic equilibrium shifts to Cage–Key association, bringing LuxSit Pro and CyOFP into close proximity with increased BRET efficiency. Dose-dependent BRET emission spectral shifts (left) were observed in response to varying concentrations of the target analyte. Dose–response curves of (B) luxPro_lucCageNPY2_330, (C) luxPro_lucCagePYY4_334, or (D) luxPro_lucCagePYY3_344 were generated in HBS buffer (middle) or 10% human pooled serum (right). The emission ratios (620/508 nm) across the target titration series were determined using 620/40 and 508/20 nm filters. LOD was calculated as 3 × $S.D._{y.x}$/slope.

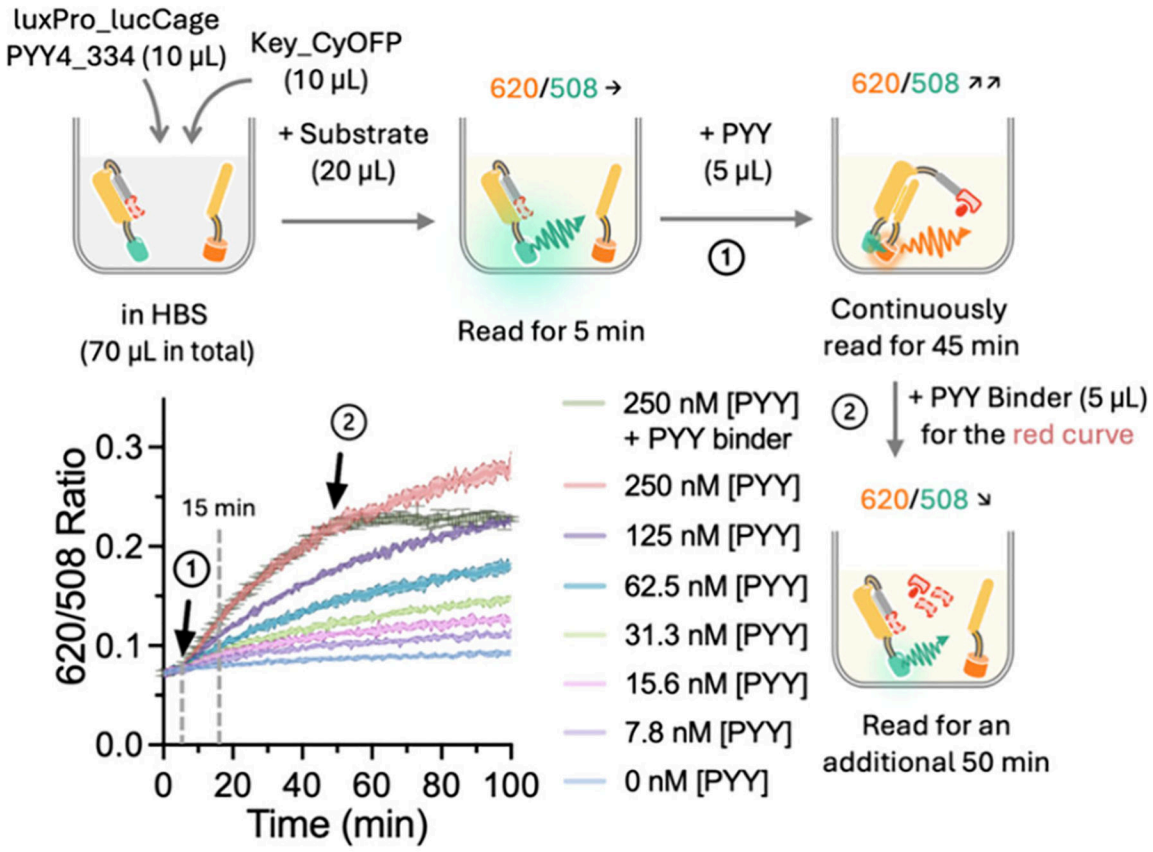

Figure 7.

Ratiometric luminescence kinetics and reversibility of luxPro_lucCagePYY4_334. Time-course ratiometric luminescence traces for luxPro_lucCagePYY4_334 are presented as 620/508 ratios, calculated from raw RLU values collected using 620/40 and 508/20 nm emission filters. Assays were performed with 5 nM luxPro_lucCagePYY4_334 and 10 nM Key_CyOFP premixed with the Luxterazine substrate in HBS buffer to measure the baseline. PYY (analyte) was added at 5 min (left arrow) to induce proximity between LuxSit Pro and CyOFP. Time-course responses are shown across a range of PYY concentrations (0–250 nM), with signals at 15 min detectable above baseline. For the 250 nM PYY condition (red curve), the 2 μM *de novo* PYY binder (green) was subsequently added at 50 min (right arrow) as a competitor to reverse the signal. Data represent mean ± s.d. from triplicate measurements.